Design of Apparatus for Ni/Mg2Si and Ni/MnSi1.75 Contact Resistance Determination for Thermoelectric Legs

Yohann Thimont, Quentin Lognoné, Christophe Goupil, Franck Gascoin, Emmanuel Guilmeau

DOI: 10.1007/s11664 013 2940 1

Design of Apparatus for Ni/Mg_2Si and Ni/$MnSi_{1.75}$ Contact Resistance Determination for Thermoelectric Legs

YOHANN THIMONT,[1,2,3] QUENTIN LOGNONÉ,[1] CHRISTOPHE GOUPIL,[1] FRANCK GASCOIN,[1] and EMMANUEL GUILMEAU[1]

1. Laboratoire CRISMAT, UMR 6508 CNRS ENSICAEN, 6, Boulevard Maréchal Juin, 14050 Caen Cedex 4, France. 2. e mail: yohann.thimont@ensicaen.fr. 3. e mail: thimont@chimie.ups lse.fr

In recent decades, thermoelectricity has been widely studied as a potential new source of renewable energy. One of the major challenges to improve the efficiency of thermoelectric (TE) devices is to minimize the contact resistance between the active material and the electrodes, since this represents the major loss of charge in a TE module. This article describes the fabrication of an apparatus for TE leg characterization built with commercial and custom-made parts based on the analog one-dimensional transmission-line method. This device permits contact resistance measurements of bulk TE legs. *p*- and *n*-type TE materials, $Mg_2Si_{0.98}Bi_{0.02}$ and $MnSi_{1.75}Ge_{0.02}$, respectively, were metallized with nickel foils and used as test materials for contact resistance characterization. Contact resistance values of 0.5 mΩ mm^2 for Ni/$Mg_2Si_{0.98}Bi_{0.02}$ junctions and 4 mΩ mm^2 for Ni/$MnSi_{1.75}Ge_{0.02}$ junctions have been measured. Contact resistance measurements are discussed depending on materials processing and the experimental measurement conditions.

Key words: Contact resistance, metal electrode, thermoelectric (TE)

INTRODUCTION

Thermoelectricity, discovered by Seebeck and Peltier in 1821 and 1834, respectively, is a phenomenon in which a temperature difference applied to a material can generate a voltage (Seebeck effect) and a temperature gradient appears when a current passes through a material (Peltier effect). Thus, devices using the Seebeck effect are used to scavenge waste energy, for example, from blast furnaces, while the Peltier effect is used to heat or cool systems such as refrigerators or car seats. Accordingly, thermoelectric (TE) converters are energy conversion devices which are characterized by their energy conversion efficiency. The efficiency of a TE device can typically be improved by increasing the figure of merit (ZT) of the materials used, defined as $ZT = S^2T/\rho\kappa$,[1] where S is the Seebeck coefficient, ρ is the electrical resistivity, κ is the thermal conductivity, and T is the temperature. In the past few decades, extensive efforts have been devoted to investigate the development of green, high-ZT TE materials. In this respect, silicide compounds such as Mg_2Si and $MnSi_{1.75}$ appear to be promising TE materials, especially when coupled with inexpensive synthesis techniques.[1–4]

Although large ZT values have been reported for different classes of materials,[5] the efficiency of TE devices is usually limited by technological issues such as heat transfer, mechanical properties, phase stability, and/or the electrical and thermal contact resistances between materials and electrodes.[6–8] The contact resistance between TE materials and metal electrodes has been investigated by McConnell and Sehr.[9] Mengali and Seiler[10] reported a contact resistance value of 1×10^{-6} Ω cm^2 in the case of copper joined to a bismuth-telluride-based thermoelement. Recently, various studies have reported contact resistances for silicide compounds such as Mg_2Si.[11] Evidently, TE materials must be metallized to obtain better contact between the legs and electronic tracks. The nature of the metal electrode plays an important role, as it must have

good affinity with the TE material, be crack-free, and have low interdiffusion (to avoid formation of secondary phases or solid solutions at the interface, which are usually detrimental to TE performance and TE module design). Finally, the resulting interface must be characterized by low thermal and electrical contact resistances so that the conversion efficiency can be optimized. Some apparatus for contact resistance measurement has been developed by Gorodetskii et al.[12] To accurately characterize the electrical contact resistance, we have also developed a new measuring system, based on the well-known contact resistance measurement method called the transmission-line method (TLM), for which detailed information can be found elsewhere.[13] We describe herein the measurement principle, apparatus design, fabrication, and example characterizations of p-type Ni/$MnSi_{1.75}Ge_{0.02}$ and n-type Ni/$Mg_2Si_{0.98}Bi_{0.02}$ nickel-plated TE legs.

THEORETICAL APPROACH OF THE MEASUREMENT PRINCIPLE

The contact resistance is determined by resistance measurements at different locations over the sample surface using a three-probe measurement technique. Resistances are determined by applying a constant current (i) between two parts of the sample holder and measurement of a voltage along the sample length as the potential difference between the probe and one side of the sample holder. The experimental procedure is presented schematically in Fig. 1.

Before each analysis, the operator must first determine the influence of the probe resistance (R_p) and the barrier potential (V_b) between the tungsten probe and the semiconductor material (diode effect).

The probe resistance R_p is deduced with the help of an optional second probe which is fixed to the apparatus and contacts the top of the TE material. Consequently, the measurement method becomes a four-probe approach. The measured total resistance is equivalent to

$$R_t = 2R_p + R_m(x),$$

where x is the distance between the two probes.

From the $R_t(x)$ curve, the y intercept is equal to $2R_p$. For Ni/Mg_2Si and Ni/$MnSi_{1.75}$ samples, the values of R_p are very low in comparison with other resistance contributions; therefore, the value of R_p can be neglected.

To determine the barrier potential V_b caused by the contact between a metal probe and a semiconductor material, current–voltage (I–V) characteristic curves are plotted for both a positive and negative voltage. For Ni/Mg_2Si and Ni/$MnSi_{1.75}$ legs, the curves obtained are symmetrical with respect to the origin and the curves pass through zero. We concluded that, for these types of TE materials, it is not necessary to take into account the barrier potential V_b in the measurement of the contact resistance.

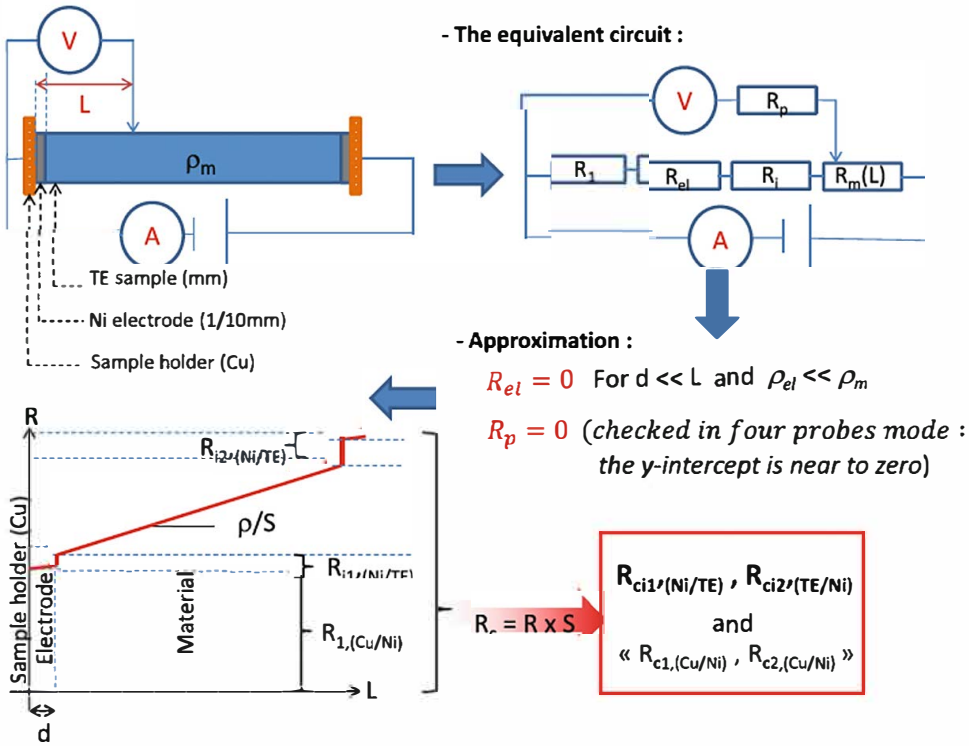

Fig. 1. Principle of the measurement technique.

The electrical circuit described by Fig. 1a is equivalent to the series of resistances presented in Fig. 1b. The measured resistance R can be expressed as follows for different locations of the probe in each of the four following defined domains:

– *Domain 1*: on top of the first electrode

$$R = R_1 + R_{\mathrm{el}},$$

where R_1 is the resistance between the sample holder and the electrode and R_{el} is the resistance of the electrode layer; $R_{\mathrm{el}} \approx 0$ because of the high conductivity of the nickel material and the fact that $d \ll L$, where d is the thickness of the electrode layer and L is the distance from the probe contact to the sample holder border, leading to the simplification

$$R = R_1.$$

– *Domain 2*: on top of the TE material

$$R = R_1 + R_{\mathrm{el}} + R_{\mathrm{i1}} + R_{\mathrm{m}}(h) + R_{\mathrm{p}},$$

where R_{i} is the contact resistance between the electrode and the TE material, h is the distance from the probe contact to the TE/metal junction of the sample, R_{m} is the resistance of the TE material as a function of h, and R_{p} is the contact resistance between the probe and the TE material, which can be approximated as

$$R(L) = R_1 + R_{\mathrm{i1}} + R_{\mathrm{m}}(h).$$

We can deduce the electrical conductivity of the TE material using the slope of the $R(h)$ curve in the domain delimited by the space between the two electrode/TE material junctions. We define

$$\rho = a \times S,$$

where a is the slope of the affine line $R(L)$.

– *Domain 3*: On top of the second electrode

$$R = R_1 + R_{\mathrm{i1}} + R_{\mathrm{m}} + R_{\mathrm{i2}}.$$

– *Domain 4*: On top of the opposite side sample holder

$$R = R_1 + R_{\mathrm{i1}} + R_{\mathrm{m}} + R_{\mathrm{i2}} + R_2.$$

Using this system of equations, we can solve for the following resistance contributions:

$$R_1, R_{\mathrm{i1}}, R_{\mathrm{i2}}, R_2.$$

The contact resistance is defined by $R_{\mathrm{c}} = R \times S$, where S is the section area of the legs; contact resistances are expressed in units of mΩ mm^2 as

$$R_{\mathrm{c1}}, R_{\mathrm{ci1}}, R_{\mathrm{ci2}}, R_{\mathrm{c2}}.$$

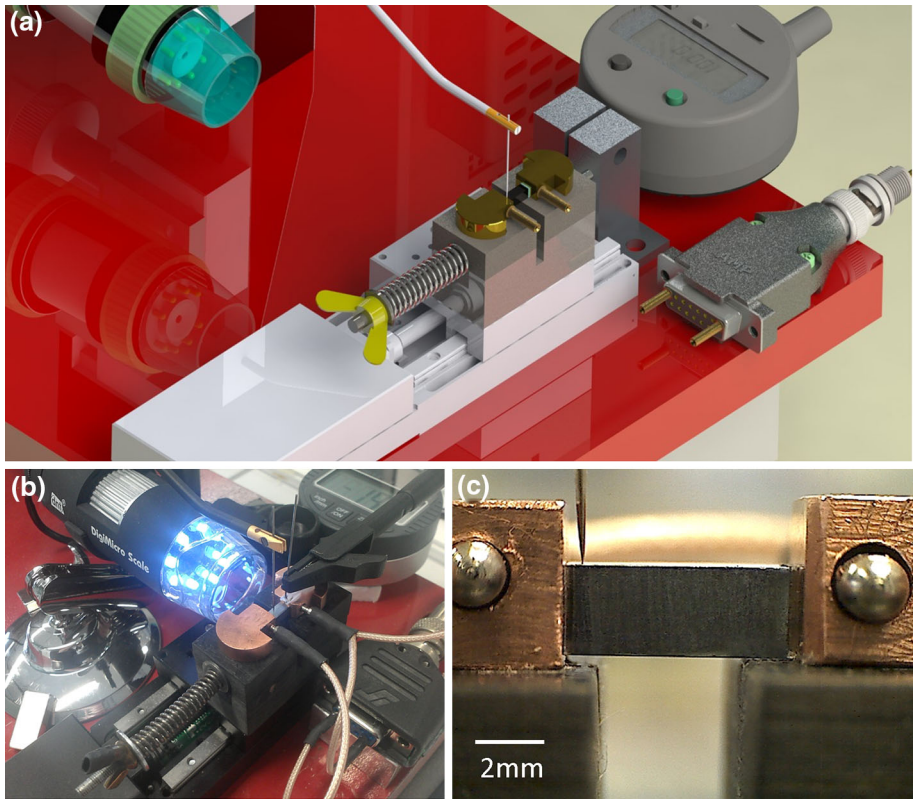

Fig. 2. (a) 3D plan of the apparatus by SolidWorks software. (b) Photograph of the apparatus. (c) Image of a Ni/Mg_2Si sample in contact with the probe through the microscope.

R_{ci1} and R_{ci2} are the interesting characteristic values for TE/metal junction characterization and TE module design.

APPARATUS FABRICATION

A custom-made contact resistance measurement apparatus built from different commercial parts such as a commercial tungsten probe (72T-J3/20K 2 μm; American Probe and Technologies Inc.) was used to obtain the potential on the top of the sample with location accuracy of 0.01 mm. A dovetail sample holder system was designed using SolidWorks software[14] then 3D printed[15] (EDEN 260). The two contact devices were machined in copper, then drilled for input/output wire connection. A spring with k = 4.528 N/mm was used to apply a controlled and permanent contact force on the sample. The spring compression was controlled by a screw characterized by spring compression of 0.5 mm/rotation, corresponding to 2.264 N/rotation. The translation motion (of the samples, with a fixed probe) is achieved via a Thorlabs MTS50/M-Z8 motorized linear rail device. The current is generated by a Keithley 6220 permanent current generator, and the potential is measured using a Keithley 2700 multimeter. A camera was also set up to carefully check the contact between the probe and the sample surface. To avoid electromagnetic perturbations, coaxial wires were used. Wires were cut as short as possible and connected using tin solder (use of indium would have led to better contacts, but the mechanical resistance of indium-based solder is significantly lower than the tin analog). The copper sample holders have an adaptive contact which allows optimization of the surface contact between the sample and the sample holder device due to a rotational degree of freedom. The technical principle of the apparatus is illustrated in Fig. 2a. The apparatus is shown in Fig. 2b, and a microscopic view (from the camera) of the probe in contact with the top of a sample is shown in Fig. 2c. The approach of the probe must be carried out carefully, and the applied pressure must be strictly limited to avoid bending of the probe in the irreversible plastic domain.

EXPERIMENTAL RESULTS

The designed apparatus was first used for characterization of 3 mm × 3 mm × 7 mm p-type $Ni/MnSi_{1.75}Ge_{0.02}$ and n-type $Ni/Mg_2Si_{0.98}Bi_{0.02}$ metallized TE legs. The samples were introduced into the sample holder device, and a permanent pressure was ensured using the compression spring. In a second time the probe location on the sample was initialized to the origin location position, locating the probe tangential to the edge of the sample holder.

The contact between the probe and sample must be accurately controlled using the screw system and was checked by means of the camera at medium magnification. No current was applied during the approach of the probe, and the open-circuit voltage (without an applied current) is near zero and stable after the contact is made. After the contact between the probe and sample is effective and stable, a permanent current of 100 mA is applied. The measured tension (without tension correction) is plotted as a function of the displacement (L). Figure 3 shows the $R(L)$ curves depending on the applied pressure. It can be noted that all the curves have the same slope, with R_m remaining the same for different applied pressures, whereas the intercept decreases with applied pressure. The contact resistance $R_{c1,Cu/Ni}$ decreases with pressure down to 0.5 MPa and remains stable up to 2 MPa.

The slope of the affine line of the experimental resistance versus length curves for any applied pressure allow us to determine an electrical resistivity of $2.19 \times 10^{5} \pm 1014 \times 10^{7}$ Ω m at

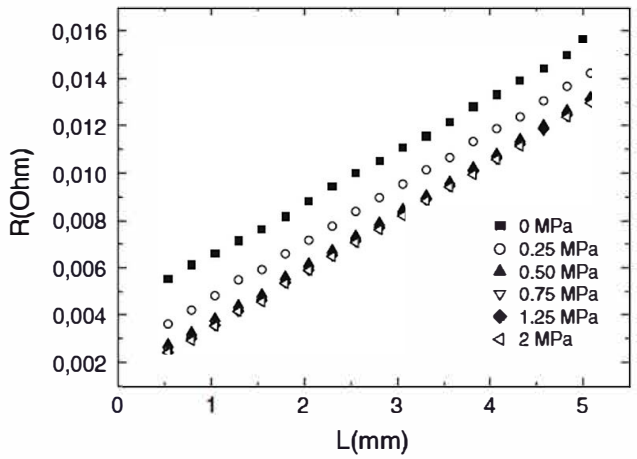

Fig. 3. $R(L)$ curves for a Ni/Mg_2Si sample for different applied pressures.

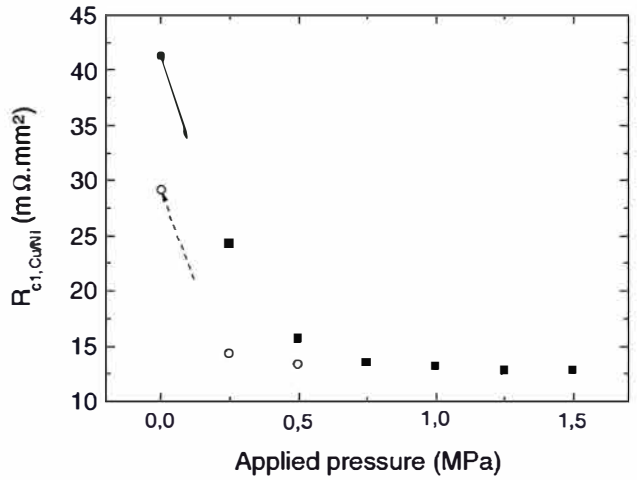

Fig. 4. Contact resistance between the sample holder and the metal electrode as a function of applied pressure; the arrow indicates rising pressure, and the dotted arrow decreasing pressure.

room temperature for the $Mg_2Si_{0.98}Bi_{0.02}$ material. This result is in agreement with results obtained by conventional four-probe measurements (ULVAC ZEM-3 system) on the same sample ($\rho = 2.136 \times 10^{-5}\ \Omega$ m). The experimental relative error of the electrical resistivity at room temperature is estimated to be about 0.5%.

Figure 4 shows the applied pressure dependence of the electrical contact resistance $R_{c1,Cu/Ni}$. The curve shows two domains: in the first part, the contact resistance decreases drastically until a pressure of 0.7 MPa is reached, whereas above this value, the contact resistance decreases slowly. Such behavior is in agreement with the work of El Abdi.[16] These results can be explained based on the Hertz model.[17] In a first step [the first part of the $R_{c1,Cu/Ni}(P)$ curve], some contacts between surface defects of the nickel electrode and surface defects of the copper sample holder are established, and the number of contacts increases with pressure, so the contact resistance decreases drastically. At higher applied pressures, no more contacts appear, but the contact area increases slowly due to plastic deformation, so the contact resistance decreases slowly, proportionally to the total contact surface area. The contact resistance between the sample holder device and the legs is very high (about 12 mΩ mm^2) in comparison with the contact resistance between the joined metal electrode layer and the TE material.

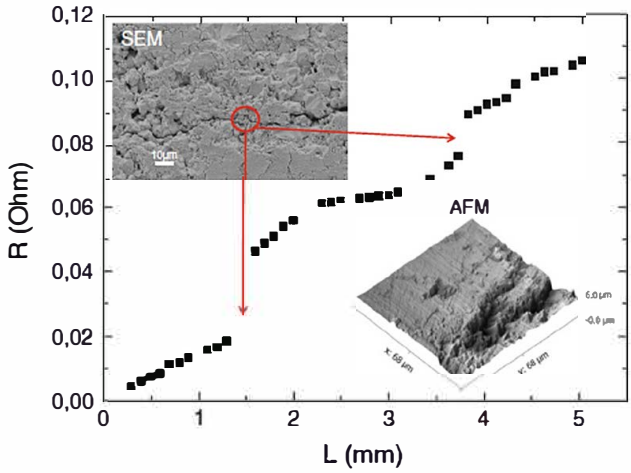

Fig. 5. Example $R(L)$ curve of a Ni/Mg_2Si microcracked sample.

Figure 5 shows the nonlinear $R(L)$ behavior of the $Mg_2Si_{0.98}Bi_{0.02}$ sample, which can be explained based on the percolation of the current flow due to the presence of intergranular microcracks in the leg. The crack topography was checked by atomic force microscopy (Fig. 5, inset), which shows a 6-μm-deep intergranular microcrack, which indeed has an important influence on the contact between the material and the probe.

The contact resistances of crack-free Ni/$Mg_2Si_{0.98}Bi_{0.02}$ and Ni/$MnSi_{1.75}Ge_{0.02}$ were measured using

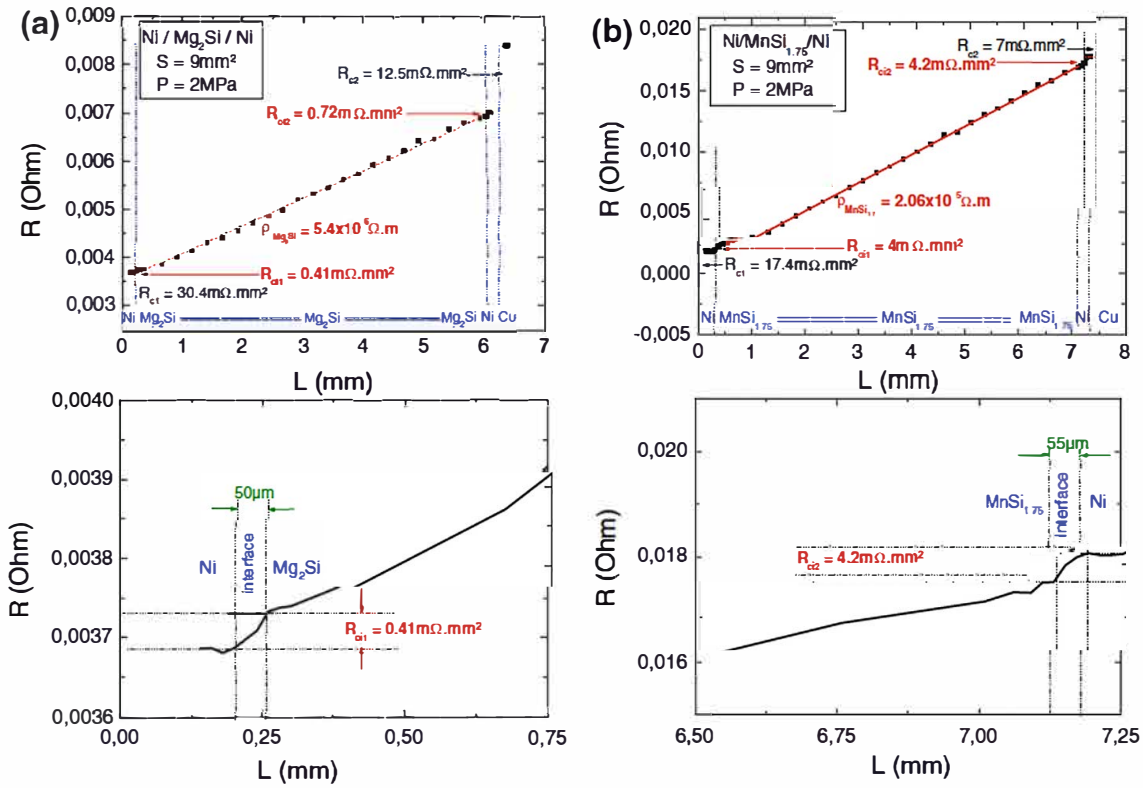

Fig. 6. $R(L)$ curves of (a) Ni/Mg_2Si and (b) Ni/$MnSi_{1.75}$ samples.

the custom-made apparatus. In fact, the contact resistances were deduced from the $R(L)$ curve by the gap electrical resistance at the junction location. We estimated the relative error to be 5% (deduced from the maximal divergence of the curve from the experimental plots).

The results are presented in Fig. 6. The average contact resistance found in the case of Ni/$Mg_2Si_{0.98}Bi_{0.02}$ was about 0.55 ± 0.03 mΩ mm^2, similar to values obtained by Sakamoto et al.[18] In the case of the $MnSi_{1.75}$/Ni junction, the average contact resistance was equal to 4.1 ± 0.2 mΩ mm^2.[19] The contact resistance between the Ni electrode and the TE material does not depend on the pressure applied on the sample holder. We also noted that the contact resistance was a function of the metallization process time. The contact resistance decreases proportionally with the interface layer thickness and the metallization process time.

CONCLUSIONS

This apparatus designed for contact resistance determination allows precise estimation of the electrical resistivity of semiconductor materials (ceramics, intermetallics) at room temperature. It also permits measurement of the influence of applied pressure on the various contact resistances via a pressure controller. $Mg_2Si_{0.98}Bi_{0.02}$ and $MnSi_{1.75}Ge_{0.02}$ TE materials show resistivity of 5.6×10^{-6} Ω m and 2.2×10^{-5} Ω m, respectively. This apparatus allows to measure the contact resistances between the joined nickel electrode layers and these TE materials do not depend on any applied pressure and also the contact resistance between the sample holder and the sample (which depend on the applied pressure).

We measured an average contact resistance for the joined nickel electrode on the TE material of 0.55 mΩ mm^2 for the Ni/$Mg_2Si_{0.98}Bi_{0.02}$ interface and 4.1 mΩ mm^2 for the Ni/$MnSi_{1.75}Ge_{0.02}$ interface.

This contact resistance determination apparatus also permits determination of the inhomogeneity of the current flow caused by intergranular microcracks. These are typically revealed by the appearance of jumps in $R(L)$ curves. Therefore, the apparatus can be employed to check the contact resistance of an assembly as well as to verify the microstructural soundness of TE legs, both of which are important aspects for TE module manufacture.

ACKNOWLEDGEMENTS

The authors thank Benoît Bougle for apparatus design by SolidWorks software and for his important involvement in the innovative technical conception of the apparatus.

REFERENCES

1. D. Berthebaud, F. Gascoin, and *J. Solid State Chem.* 202, 61 (2013).
2. M. Iannou, K. Chrissafis, E. Pavlidou, F. Gascoin, and Th Kyratsi, *J. Solid State Chem.* 197, 172 (2013).
3. S.M. Choi, K. H. Kim, I. H. Kim, S. U. Kim, and W. S. Seo, *Curr. Appl. Phys.* 11, 388 (2011).
4. I. Aoyama, M.I. Fedorov, V.K. Zaitsev, FYu Solomkin, I.S. Eremin, A.Y. Samunin, M. Mukoujima, S. Sano, and T. Tsuji, *Jpn. J. Appl. Phys.* 44, 8562 (2005).
5. E. Savary, F. Gascoin, and S. Marinel, *Dalton Trans.* 39, 11074 (2010).
6. H. Matino and M. Tokunaga, *J. Electrochem. Soc.* 116, 709 (1969).
7. W. Edwards, *Solid State Electron.* 15, 387 (1972).
8. C. N. Liao, C. H. Lee, and W.J. Chen, *Electrochem. Solid State* 10, 23 (2007).
9. G. McConnell and R. Sehr, *Solid State Electron.* 2, 157 (1961).
10. O.J. Mengali and M.R. Seiler, *VDI Berichte* 2, 59 (1962).
11. T. Sakamoto, K. Sugiyama, D. Mori, M. Ogi, K. Nishio, Y. Kogo, Y. Takanashi, and T. Iida, *AIP Conf. Proc.* 1449, 223 (2012).
12. S.M. Gorodetskii, I.A. Drabkin, and I.V. Nelson, *Ind. Lab+.* 56, 820 (1991).
13. H.H. Berger, *Solid State Electron.* 15, 145 (1972).
14. SolidWorks software, http://www.solidworks.com.
15. L. Manolis Sherman, *Plast. Technol.* (2004).
16. R. El Abdi and N. Benjemaa, *Int. J. Syst. Appl.* 2, 75 (2008).
17. H.R. Hertz, *J. Reine. Angew. Math.* 92, 156 (1881).
18. T. Sakamoto, T. Lida, Y. Honda, M. Tada, T. Sekiguchi, K. Nishio, Y. Kogo, and Y. Takanashi, *J. Electron. Mater.* 41, 1805 (2012).
19. X. Shi, Z. Zamanipour, and D. Vashaee, *APS J.*, March Meeting 56 (2011).